Constant Property Newtonian Fluid Flow and Heat Transfer overCascaded Fins

Y. Menni, A. Azzi and C. Zidani

Unit of Research on Materials and Renewable Energies, URMER
Department of Physics, Faculty of Sciences,
Abou Bekr Belkaid University, B.P. 119, 13000 Tlemcen, Algeria

(reçu le 10 Novembre 2016 - attaché le 25 Mars 2017)

Abstract - *Turbulent flow and heat transfer characteristics were studied and analyzed numerically for a constant property Newtonian fluid flowing through a two-dimensional horizontal rectangular cross section channel with staggered, transverse cascaded rectangular-triangular fins (CRTFs) and a constant temperature along both walls. The governing equations based on k-ε model used to describe the turbulence phenomenon, are solved by the finite volume method using the SIMPLEC-algorithm. Computations were carried out in the fully-developed regime for different Reynolds numbers, and geometric locations. In particular, velocity and temperature fields, skin friction coefficient, and local and average Nusselt numbers were obtained. This study can be a real application in the field of heat exchangers and air plane solar collectors.*

Résumé – *Des caractéristiques d'écoulement turbulent et de transfert thermiques sont étudiées et analysées numériquement pour un fluide Newtonien à propriétés constantes qui s'écoule à travers une conduite bidimensionnelle horizontale de section rectangulaire avec des ailettes en cascade 'rectangulaire-triangulaire' (CRTFs), transverses et étagées et une température uniforme le long des parois. Les équations gouvernantes, basées sur le modèle k-ε est employé pour modéliser la turbulence, sont résolues par la méthode des volumes finis en utilisant l'algorithme SIMPLEC. Des calculs sont menés dans le régime pleinement développé pour différents nombres de Reynolds, et différentes locations géométriques. En particulier, les champs de vitesse et de température, l'évolution du coefficient de friction, ainsi que et les distributions local et moyen du nombre de Nusselt ont été obtenus. Cette étude peut être une application réelle dans le domaine des échangeurs de chaleur et les capteurs solaires plans à écoulement d'air.*

Keywords: Cascaded fin - Heat transfer - Numerical simulation - Rectangular channel.

1. INTRODUCTION

The flow separation in ducts with segmented baffles has many engineering applications, for example, shell-and-tube heat exchangers with segmented baffles, labyrinth shaft seals, laser curtain seals, air-cooled solar collectors, and internally cooled turbine blades [1].

In the literature, different shapes, orientations and locations of the baffles in heat exchangers have been the subject of several scientific studies. The first work on the numerical investigation of flow and heat transfer characteristics in a duct with the concept of periodically fully developed flow was conducted by Patankar *et al.* [2]. Founti *et al.* [3] used the Laser Doppler Anemometry measurement technique to derive the velocity field in a shell-and-tube heat exchanger with transverse baffles. The similar distributions of the mean flow velocity and turbulent intensity were found after two sets of baffles from the channel entrance.

In addition, Berner *et al.* [4, 5] obtained experimental results of velocity and turbulence mean distributions in flow around segmented baffles using the Laser Doppler Anemometry measurement technique. The objective was to determine the number of baffles necessary for obtaining a periodic boundary condition and the dependence on Reynolds number and the geometry.

Antoniou *et al.* [6] analyzed the flow over prisms with several aspect ratios using hot wire technique. Habib *et al.* [1] reported the characteristics of turbulent flow and heat transfer inside the periodic cell formed between segmented baffles staggered in a rectangular duct and pointed out that the pressure drop increases with the baffle height.

Three different baffle arrangements were considered. Their results showed that a significant heat transfer enhancement in a heat exchanger tube can be achieved by introducing a baffle inclined towards the downstream side, with the minimum pressure loss. Thermal and hydrodynamic parameters were examined numerically and experimentally by Lei *et al.* [18] for a flow passing through a channel with only one helicoidal baffle. A comparative study between three different channels was conducted by the investigators.

In the first case, a channel without any baffles was examined. In the second case, the same channel with only one helicoidal baffle was examined. In the third case, the same channel with two helicoidal baffles was examined. Another experimental investigation was carried out by Karwa *et al.* [19] to evaluate teat transfer and friction in an asymmetrical heated rectangular duct with half and fully perforated baffles at different pitches. Results showed that the half perforated baffles are thermo-hydraulically better to the fully perforated baffles at the same pitch. They also showed that the half perforated baffles at a relative roughness pitch of 7.2 give the greatest performance advantage of 51.6-75% over a smooth duct at equal pumping power.

Promvonge [20] made an experimental study to assess turbulent forced convection heat transfer and friction loss behaviors for airflow through a channel fitted with a multiple 60° V-baffle turbulators. Experimental results show that the V-baffle provides the drastic increase in Nusselt number, friction factor and thermal enhancement factor values over the smooth wall channel due to better flow mixing from the formation of secondary flows induced by vortex flows generated by the V-baffle.

The forced convection heat transfer and pressure drop for a horizontal cylinder with vertically attached imperforate and perforated circular fins experimentally investigated by Karabacak *et al.* [21]. They showed in the cases of the Re above the critical value that Nusselt numbers for the perforated finned positions are 12 % higher than the Nusselt numbers for the imperforate state. They also showed a correlation between the Re and Nu in the Re number above the critical value and the Re below the critical value. Meanwhile, correlations regarding pressure drops in the flow areas have been obtained.

Recently, Sriromreun *et al.* [22] carried out a numerically and experimentally study on heat transfer enhancement in a channel with baffle turbulators placed in a zigzag shape (Z-shaped baffle) aligned in series on the isothermal-fluxed top wall, similar to the absorber plate of a solar air heater channel. Experimental results showed a significant effect of the presence of the Z-baffle on the heat transfer rate and friction loss over the smooth channel with no baffle.

As well as the Nusselt number, friction factor and thermal performance enhancement factor for the in-phase 45° Z-baffles are found to be considerably higher than those for the out-phase 45° Z-baffle at a similar operating condition. Another numerical and experimental investigation was carried out by Ary *et al.* [23] to evaluate effect of a number of inclined perforated baffles on the flow patterns and heat transfer in a rectangular channel with different types of baffles.

Results showed that the flow patterns around the holes are entirely different with different numbers of holes and it significantly affects the local heat transfer, and two baffles provide greater heat transfer performances than a single baffle.

The shell-and-tube heat exchangers are used in several sectors and in very diverse fields. The improvement of their performance has been and still is the concern of

theorists and practitioners. Thus it is important to examine the design of an obstacle for this flow geometry and its impact on the heat transfer enhancement. This is the motivation for the present study, in which we reported a detailed CFD simulation of the fin design and its impact on the heat transfer phenomenon in a constant temperature-surfaced rectangular cross section channel.

2. MATHEMATICAL MODEL

A computational fluid dynamical analysis of the forced-convection heat transfer in a two-dimensional horizontal rectangular channel is reported. Two staggered, transverse, cascaded rectangular-triangular, solid-type fins (CRTFs) are introduced in the channel to produce vortices to enhance mixing and thus, the heat transfer. A schematic view of the concerned geometry with the cascaded baffles and boundary conditions is shown in figure 1.

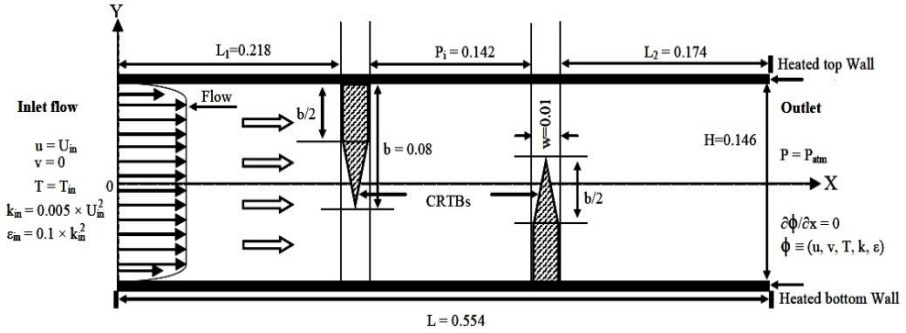

Fig. 1: Channel geometry with the CRTBs
and boundary conditions (dimensions in m)

The numerical model for air flow in the cascaded baffled channel was developed under the following assumptions: (i) the forced-heat transfer flow is steady, two-dimensional, turbulent and incompressible, (ii) Physical properties of fluid (air) are constant, (iii) Velocity profile at the inlet is uniform, (iv) Negligible radiation heat transfer, and (v) Buoyancy effects are assumed negligible.

Based on above assumptions, the governing flow equations used to simulate the fluid flow and heat transfer in the given computational domain are given as:

Continuity equation

$$\frac{\partial}{\partial x_i}(\rho u_i) = 0 \tag{1}$$

Momentum equation

$$\frac{\partial}{\partial x_i}(\rho u_i u_j) = \frac{\partial}{dx_i}\left(\mu\left(\frac{\partial u_i}{\partial x_j} - \rho\overline{u_i' u_j'}\right)\right) - \frac{\partial P}{\partial x_i} \tag{2}$$

where ρ is the fluid density; P the pressure; μ dynamic viscosity; u_i and u_j are mean velocity components in x_i and x_j directions.

Energy equation

$$\frac{\partial}{\partial x_i}(\rho u_i T) = \frac{\partial}{\partial x_i}\left((\Gamma + \Gamma_t)\frac{\partial T}{\partial x_j}\right) \tag{3}$$

where Γ and Γ_t are molecular thermal diffusivity and turbulent thermal diffusivity, respectively and are given by

$$\Gamma = \mu / Pr \qquad \text{and} \qquad \Gamma_t = \mu_t / Pr_t \tag{4}$$

In {Eq. (2)}, $\rho\overline{u_i' u_j'}$ is the additional term of Reynolds stresses due to velocity fluctuations, which has to be modelled for the closure of {Eq. (2)}. The classical approach is the use of Boussinesq hypothesis, relating Reynolds stresses and mean flow strain, through the eddy viscosity concept [24]. In its general formulation, as proposed by Kolmogorov, Boussinesq hypothesis is written as,

$$-\rho\overline{u_i' u_j'} = \mu\left(\frac{\partial u_i}{\partial x_i} + \frac{\partial u_j}{\partial x_j}\right) - \frac{2}{3}\left(\rho_k + \mu_t \frac{\partial u_i}{\partial x_j}\right)\delta_{ij} \tag{5}$$

where δ_{ij} is the Kroenecker delta and μ_t the eddy viscosity defined as,

$$\mu_t = \rho C_\mu \frac{k^2}{\varepsilon} \tag{6}$$

The standard $k-\varepsilon$ model is an example of the two-equation models that use the Boussinesq hypothesis, details of which can be found in Launder and Spalding [25]. The standard $k-\varepsilon$ model is defined by two transport equations, one for the turbulent kinetic energy, k and the other for the specific dissipation rate ε, as given below,

$$\frac{\partial}{\partial x_j}(\rho k u_j) = \frac{\partial}{\partial x_j}\left((\mu + \frac{\mu_t}{\sigma_k})\frac{\partial k}{\partial x_j}\right) + G_k + \rho\varepsilon \tag{7}$$

$$\frac{\partial}{\partial x_j}(\rho \varepsilon u_j) = \frac{\partial}{\partial x_j}\left((\mu + \frac{\mu_t}{\sigma_\varepsilon})\frac{\partial \varepsilon}{\partial x_j}\right) + C_{1\varepsilon}\frac{\varepsilon}{k} - C_{2\varepsilon}\rho\frac{\varepsilon^2}{k} \tag{8}$$

In these equations, G_k represents turbulence kinetic energy generated by the mean velocity gradients. The empirical constants for the standard *k-ε*model are assigned the following values [25]: $C_\mu = 0.99$; $C_{1\varepsilon} = 1.44$; $C_{2\varepsilon} = 1.92$; $\sigma_k = 1.0$ and $\sigma_\varepsilon = 1.3$.

The Reynolds number is taken according to the experiment of Demartini *et al.* [15], it is equal to 8.73×104. This dimensionless parameter is defined as,

$$Re = \frac{\rho \overline{U} D_h}{\mu} \tag{9}$$

where $\overline{U}$ is the inlet average velocity of the channel and D_h is the hydraulic diameter, which is expressed as follows,

$$D_h = 4HW / 2(H+W) \tag{10}$$

The skin friction coefficient is given by,

$$C_f = \frac{2\,\tau_w}{\rho\,\overline{U}^2} \tag{11}$$

The numerical friction factor was evaluated from the pressure drop, ΔP across the computational domain, using Darcy Weisbach formula. That is,

$$f = \frac{(\Delta P / L)\,D_h}{1/2\,\rho\,\overline{U}^2} \tag{12}$$

The heat transfer is measured by the local Nusselt number which can be written as,

$$Nu_x = \frac{h_x\,D_h}{\lambda_f} \tag{13}$$

The average Nusselt number can be obtained by,

$$Nu = \frac{1}{L}\int Nu_x\,dx \tag{14}$$

where h_x is the local convective heat transfer coefficient.

We then present the boundary conditions. The hydrodynamic boundary conditions are set according to the numerical and experimental work of Demartini *et al.* [15]. The thermal boundary conditions are chosen according to the numerical and experimental work of Nasiruddin *et al.* [17]. A uniform one-dimensional velocity is applied as the hydraulic boundary condition at the inlet of the computational domain, as shown in figure 1.

The physical properties of air are constant. No-slip wall condition is applied for the channel walls and the baffles. A constant temperature of 375 K was applied on the walls of the channel as the thermal boundary condition. The temperature of the working fluid was set equal to 300 K at the inlet of the channel. In the channel exit it is prescribed the atmospheric pressure.

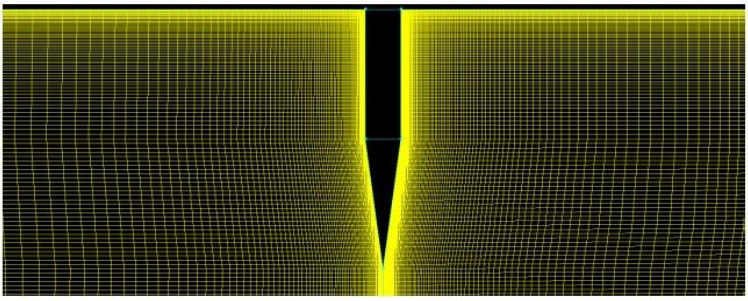

Fig. 2: Mesh generated on the first CRTF with refinements near the solid boundary

3. CFD SIMULATION

Investigations are achieved via numerical simulations by using the Commercial CFD software Fluent 6.3. The channel flow model is governed by the Reynolds Navier-Stokes (RANS) equations with the Standard $k-\varepsilon$ turbulence model [25] and the energy equation.

All the equations are discretized by the finite volume method [26] and SIMPLEC [27] algorithm is implemented. The convective terms in governing equations are discretized by QUIK numerical scheme [28]. A structured, quadrilateral, non-uniform mesh with refinements near the all solid boundaries in the two directions is employed (figure 2).

This refinement was necessary to resolve the strong velocity and temperature gradients in those regions. To examine the effect of the grid size on the CFD solution, different grid systems are tested and a grid system of 215.85 in X and Y directions, respectively, is chosen is view of saving computation time.

The convergence criterion is that the normalized residuals are less than 10^{-7} for the flow equations and 10^{-9} for the energy equation.

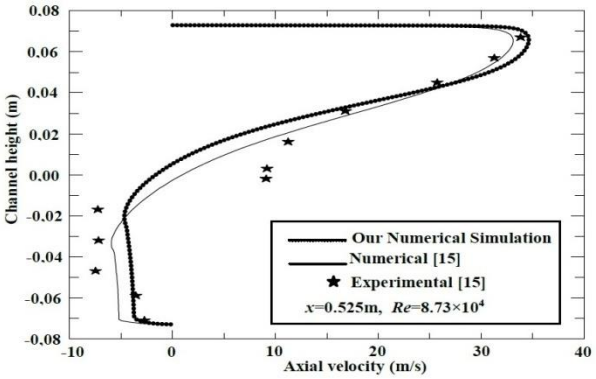

Fig. 3: Validation plot of the axial velocity distribution with experimental data [15]

To verify our numerical solution, comparison is made with the numerical and experimental data obtained by Demartini *et al.* [15]. In that study, the flow through a rectangular channel, where two baffle plates were placed in opposite walls, was analyzed.

The geometry of the problem is a simplification of the geometry of baffle plates found in shell-and-tube heat exchangers. The comparison is shown in figure 3 for validation of the axial velocity at $x = 0.525\,\mathrm{m}$ for $\mathrm{Re} = 8.73\times10^4$. The results show a good agreement between the numerical and experimental data.

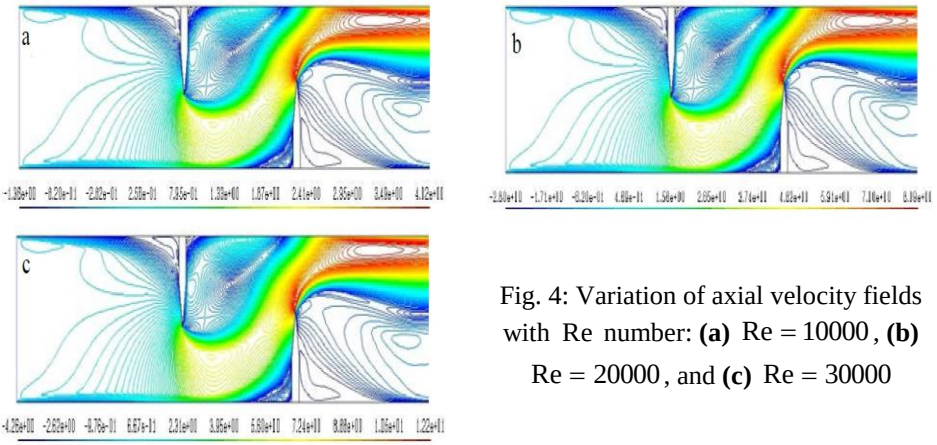

Fig. 4: Variation of axial velocity fields with Re number: **(a)** $\mathrm{Re} = 10000$, **(b)** $\mathrm{Re} = 20000$, and **(c)** $\mathrm{Re} = 30000$

4. RESULTS AND DISCUSSION

The fluid circulates inside a channel of rectangular section, containing two CRTFs. The channel with CRTF inserts can serve as an effective application for enhancing heat transfer. This is an important problem in the scope of heat exchangers where the characterization of the fluid flow as well as the existence and the extension of possible recirculation need to be identified [15].

Air is the working fluid with the flow rate in terms of Reynolds numbers ranging from 10 000 to 30 000. The velocity for and temperature fields as well as the friction loss and Nusselt number distributions are presented a typical case and for the representative value of Reynolds Number.

The impact of the CRTFs on the structure of the near wall flow is shown in figure 4. The contour plots in figure 4 present the axial velocity fields along the length of the channel at different values of Reynolds number. In all cases, the influence of the deviation of the flow field increases as the flow approaches the first CRTF, increasing the velocity of the flow approaching the passage under the fin. In the intermediate zone, the flow is characterized by very high velocities at the lower part of the channel, approaching 293-884 % of the inlet velocity, which is 0.918 m/s, depending on the Re values.

In the upper part of the channel, negative velocities indicate the presence of recirculation behind the first CRTF. In the regions upstream of the second CRTF, the plots show that as the flow approaches the second fin, its velocity is reduced in the lower part of the channel, while in the upper part, the flow starts to accelerate toward the gap above the second CRTF.

Downstream of the second CRTF, The greatest values occur, as expected, near the upper wall of the channel. These values are only possible due to the very strong flow recirculation on the back side of the second CRTF, which leads air from outside of the channel into the test section. These results seem consistent with those obtained experimentally by Demartini *et al.* [15].

The comparison of axial velocity fields at different Reynolds numbers shows that as the flow is accelerated and redirected near the CRTFs, a very small recirculation zone is formed in the vicinity of the upper left corner.

In the region downstream, a strong recirculation zone is observed, which was induced due to the flow separation. The recirculation zone was located close to the solid wall and its height was approximately equal to the extent of the flow blockage by the CRTF, which is equal to 0.08 m for all cases shown in figure 4.

A similar phenomenon is observed near the CRTF mounted on the lower wall of the channel with recirculation cells at the upstream and downstream fin. These observations are confirmed by the works of research of Nasiruddin *et al.* [17], and Pirouz *et al.* [29].

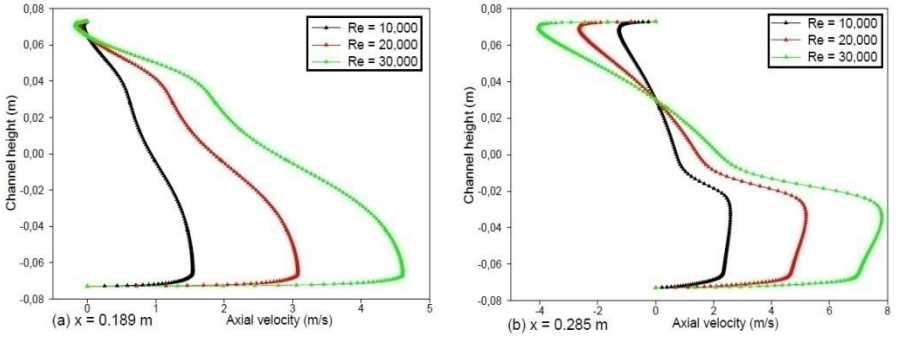

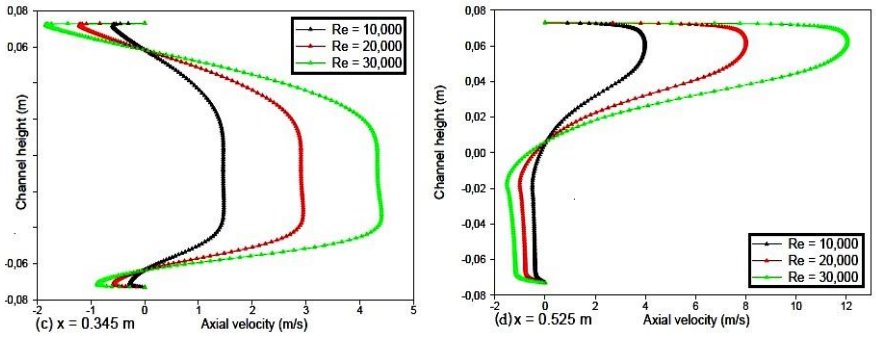

Fig. 5: Variation of axial velocity with Re number for different stations **(a)** x = 0.189 m, **(b)** x = 0.285 m, **(c)** x = 0.345 m, and **(d)** x = 0.525 m

The axial velocity profile plots for positions x = 0.189, 0.285, 0.345, and 0.525 m, measure downstream of the inlet, are shown in figure 5**a-**, **b-**, **c-**, and **d-**, respectively. Here the axial velocity profiles around the CRTFs are shown as a function of Re number (Re = 10000, 20000, and 30000).

It is observed from this figure that the flow is accelerating in its main direction from left towards right-hand side by increasing the recirculation zones (negative sense) hence the length of these cells of recycling is proportional to the increase in the flow Reynolds number.

The presence of the CRTFs influences not only the velocity field but also the pressure distribution in the whole domain investigated, as indicated by Demartini *et al.* [15]. The contour plots of dynamic pressure filed (P_d) are shown for Re = 10 000, 20 000, and 30 000 in figure 6**a-**, **b-**, and **c-**, respectively.

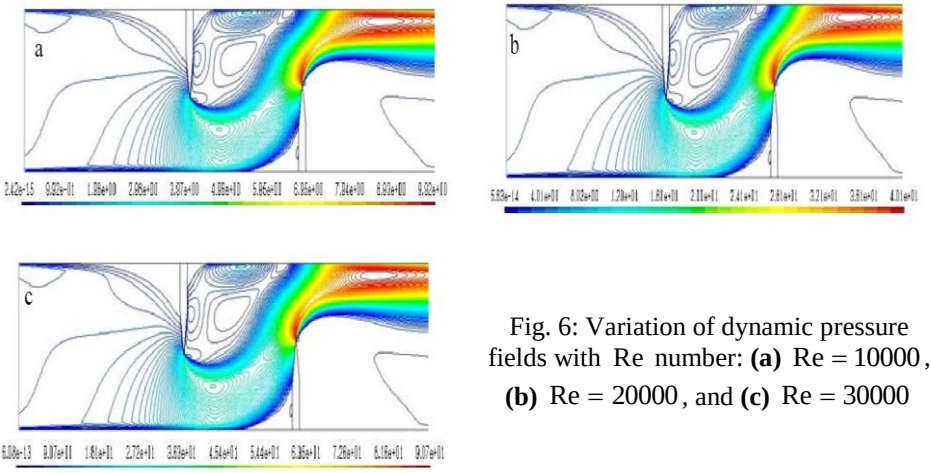

Fig. 6: Variation of dynamic pressure fields with Re number: **(a)** Re = 10000, **(b)** Re = 20000, and **(c)** Re = 30000

It is clear from these contours and their scales that the P_d increases with the increase of Re number, as expected. The plots show very low P_d values adjacent to the CRTFs.

Downstream of the considered CRTFs, recirculation cells with very low P_d values are observed. In the regions between the tip of the CRTFs and the channel walls, the P_d is increased.

Similarly to the results in figure 4, the highest P_d values are found near the top wall of the channel with an acceleration process that starts just after the second CRTF, in according with the results by Demartini *et al.* [15].

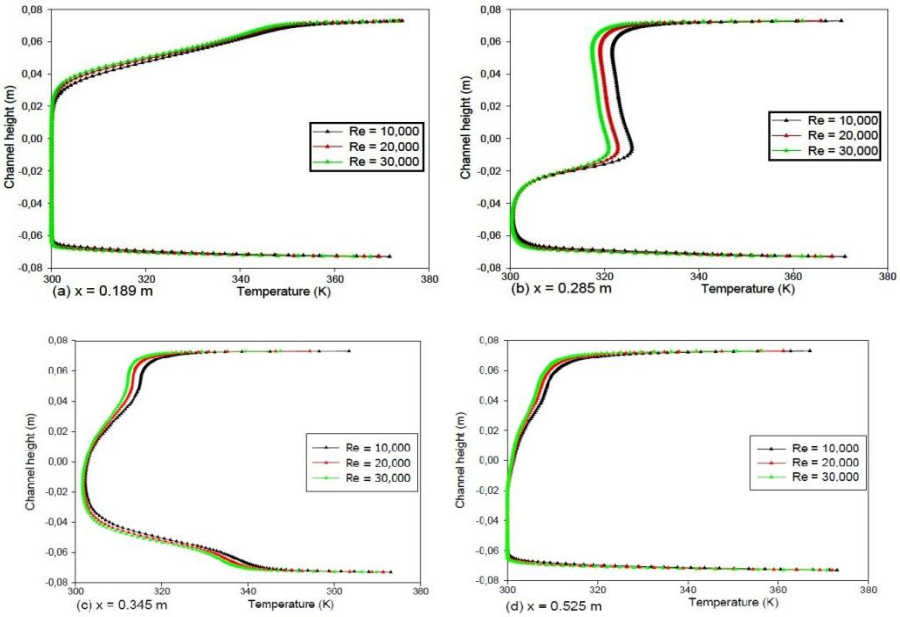

Fig. 7: Variation of temperature with Re for different stations
(**a**) x = 0.189 m, (**b**) x = 0.285 m, (**c**) x = 0.345 m, and (**d**) x = 0.525 m

The temperature repartition is also affected by the presence of the CRTFs as it appears in figure 7. As expected, the largest variations in the fluid temperature occur in the region near to the CRTFs. The plots show that the fluid temperature in the recirculation regions is significantly high as compared to those in the same regions of no baffle case.

This results show the same behavior as Nasiruddin *et al.* [17] results. The lower temperature values in the regions between the tip of the CRTFs and the channel walls are due to the high velocities in those regions. What was also noticed, the temperature value tends to decrease with the rise of Reynolds number values for all locations.

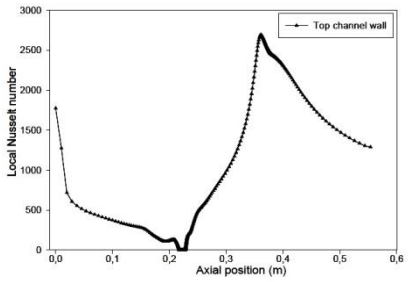

Fig. 8: Variations of local Nusselt number along the heated top channel wall for Re = 10000

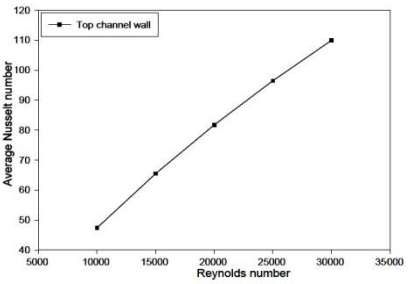

Fig. 9: Variations of average Nusselt number with Re number at the surface of the heated top wall

Figure 8 shows the numerical results of local Nusselt number (Nu_x) distributions at the heated top wall of the channel when $Re=10000$ .Similar to the results in [31], the Nu_x profiles show the largest value in the region opposite the second CRTF and the smallest value in the region around the first CRTF. The Nu_x values tend to drop considerably to almost zero when it reaches and passes the first CRTF. In the region downstream of the first CRTF, the Nu_x value is enhanced.

This enhancement is due to the intense mixing by the recirculation, as indicated by Nasiruddin *et al.* [17]. As expected, the highest Nu_x values are found near the tip of the second CRTF, due to the strong temperature gradients in that region.

The impact of Reynolds number on the average Nusselt number (Nu) is presented in figure 9 where it is shown an increase of the Nu value by increasing Re number due to the augmentation of the inertia forces further to augmentation of the flow rate. These results show the same comportment as Guerroudj *et. al.* [30].

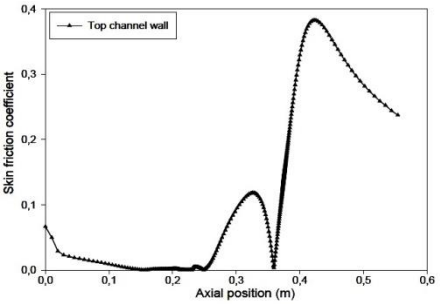

Fig. 10: Variations of skin friction coefficient along the heated top channel wall for $Re=10000$

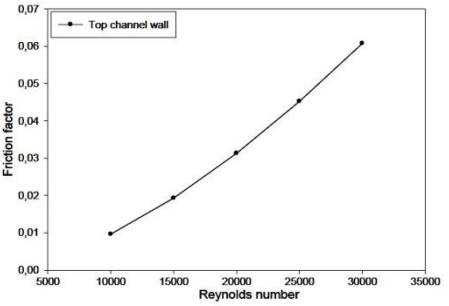

Fig. 11: Variation of friction factor with Re number at the surface of the heated top wall

The heat transfer behavior alone does not provide a complete evaluation of thermal performance. The increase in friction loss, which is a measure of the energy required by the system, must be weighed against the improvement in heat transfer for each fin configuration. This optimisation process is critical for improving energy efficiency and comparing the contrast between heat exchanger gains and losses [32].

Skin friction coefficient (C_f) is calculated from their definition as given in {Eq. (11)}. The peak C_f can be observed at the region opposite the second CRTF while the lowest of the C_f is found at the region around the first CRTF. However, the C_f values are increased again at the locations corresponding to the zone of recirculation behind the first CRTF as seen in the figure 10.

Figure 11 shows the friction factor (f) versus the Reynolds number for the channel with CRTFs. In the figure, the f values are related as a function of Re number. It is clear from this figure that the f value increases with the increase of Re , as expected.

5. CONCLUSION

A computational fluid dynamical analysis of the turbulent heat transfer in a two-dimensional horizontal rectangular cross section channel has been reported. Two cascaded rectangular-triangular fins (CRTFs) were introduced into the field to produce recirculation cells to enhance mixing and thus, the thermal performance.

The channel flow model was governed by the Reynolds averaged Navier-Stokes (RANS) equations with the standard $k-\varepsilon$ turbulence model and the energy equation. All the equations are discretized by the QUICK scheme and SIMPLEC-algorithm was implemented.

The flow pattern is affected by the presence of these fins, resulting in the formation of recirculation zones downstream from each CRTF. Due to the changes in the flow direction produced by the CRTFs, the highest velocity and dynamic pressure values appear near the upper channel wall with an acceleration process that starts just after the second CRTF, in accordance with the results by Demartini *et al.* [15].

The temperature profiles obtained for different axial stations in the channel show that the fluid temperature in the region of recirculation is significantly high as compared to that in the same region of no baffle cases, as reported by Nasiruddin *et al.* [17]. The highest temperature gradients are found in the regions between the tip of CRTF and the wall of the channel, due to the high velocity in that region, and in general, both the Nusselt number and the friction factor increase with increasing flow Reynolds number.

The computational results were compared with those obtained by the experiment in the literature. This comparison shows that there is a qualitative agreement as well as a very good concordance between the two results. This study can be a real application in the field of shell-and-tube heat exchangers and air plane solar collectors.

NOMENCLATURE

a , Triangular baffle height, m	b , Cascaded baffle height, m
C_f , Skin friction coefficient	C_p , Specific heat at constant pres., kJ/kg K
$C_{1\varepsilon}$, Empirical constant used in the standard k-*å* model	$C_{2\varepsilon}$, Empirical constant used in the standard k-*å* model
Re , Reynolds number based on the channel hydraulic diameter	G_k , Production of turbulent kinetic energy, m^2/s^2
H , Channel height, m	f , Friction factor
h_x , Local convective heat transfer coefficient, $W/m^2.K$	L , Length of rectangular channel in x-direction, m.
L , Length of rectangular channel in x-direction, m	L_2 , Distance downstream of the second baffle, m
$\overline{Nu}$, Average Nusselt number	Nu_x , Average Nusselt number
ΔP , Pressure drop, Pa	P , Pressure, Pa
P_{atm} , Atmospheric pressure, Pa	P_i , Baffle distance or spacing, m
L_1 , Distance upstream of the first baffle, m	Pr , Molecular Prandtl number
Pr_t , Turbulent Prandtl number	S , Modulus of the mean rate-of- strain tensor
T , Temperature, °C	T_{in} , Inlet temperature, °C
T_w , Wall temperature, °C	U_{in} , Inlet velocity, m/s
$\overline{U}$, Mean axial velocity of the section, m/s	u , fluid velocity in *x*-direction, m/s
u_i , u_j , Mean velocity component in *xi*-, *xj*-direction, m/s	u_i' , u_j' , Fluctuation velocity component in *xi*-, *xj*- direction, m/s
v , fluid channel width velocity in *y*-direction, m/s	W , Channel width, m

w , cascaded fin thickness, m	x , y , Cartesian coordinates, m
ε , Specific dissipation rate, m^2/s	κ , Von Karman constant, (0.4187)
Γ , Molecular thermal-diffusivity, kg/m.s	Γ_t , Turbulent thermal-diffusivity, kg/m.s
δ_{ij} , Kronecker delta	ρ , Fluid density, kg/m^3
λ_f , Fluid thermal conductivity, W/m.°C	λ_s , Solid thermal conductivity, W/m.°C
μ , Molecular viscosity, kg/m.s	μ_t , Eddy viscosity, kg/m.s
σ_k , Turbulent Prandtl number for *k*-equation	σ_ε , Turbulent Prandtl number for ε-equation
τ_w , Wall shear stress, kg/s^2m	ϕ , stands for the dependent variables u, v, k, ε and T
Atm, atmospheric ; f, fluid ; s, solid ; w, wall	in, inlet of the computational domain ;
i,j, refers coordinate direction vectors ;	x, local ; t, turbulent
w, mur ;	

REFERENCES

[1] M.A. Habib, A.M. Mobarak, M.A. Sallak, E.A. Abdel Hadi and R.I. Affify, *'Experimental Investigation of Heat Transfer and Flow Over Baffles of Different Heights'*, Transactions ASME Journal of Heat Transfer, Vol. 116, N°2, pp. 363-368, 1994.

[2] S.V. Patankar, C.H. Liu, E.M. Sparrow, '*Fully Developed Flow and Heat Transfer in Ducts Having Streamwise-Periodic Variations of Cross-Sectional Area*', Trans ASME J Heat Transfer, Vol. 99, pp. 180-186, 1977.

[3] M.A. Founti, J.H. Whitelaw, *'Shell Side Flow in a Model Disc and Doughnut Heat Exchanger*', Tech. Report FS/81/37. Mech. Eng. Dept., Imperial College, London, UK, 1981.

[4] C. Berner, F. Durst and D.M. McEligot, *'Flow Around Baffles'*, Journal of Heat Transfer, Vol. 106, N°4, pp. 743 - 749, 1984.

[5] C. Berner, F. Durst, D.M. McEligot, *'Streamwise-Periodic Flow Around Baffles'*. In: Proceedings of the 2nd international conference on applications of laser anemometry to fluid mechanics', Lisbon, Portugal, 1984.

[6] J. Anotoniou and G. Bergeles, *'Development of the Reattached Flow Behind Surface-Mounted Two-Dimensional prisms'*, Journal of Fluids Engineering, Vol. 110, N°2, pp. 127 - 133, 1988.

[7] H. Li and V. Kottke, *'Effect of Baffle Spacing on Pressure Drop and Local Heat Transfer n Staggered Tube Arrangement'*, International Journal of Heat and Mass Transfer, Vol. 41, N°10, pp. 1303-1311, 1998.

[8] H. Li and V. Kottke, '*Visualization and Determination of Local Heat Transfer Coefficients in Shell-and-Tube Heat Exchangers for Staggered Tube Arrangement by Mass Transfer Measurements*'. Experimental Thermal Fluid, Vol. 17, N°3, pp. 210-216, 1998.

[9] H. Li and V. Kottke, *'Analysis of Local Shell-Side Heat and Mass Transfer in The Shell-and-Tube Heat Exchanger With Disc and-Doughnut Baffles'*, International Journal Heat and Mass Transfer, Vol. 42, pp. 3509 - 3521, 1999.

[10] H. Li and V. Kottke, *'Effect of the Leakage on Pressure Drop and Local Heat Transfer in Shell-and-Tube Heat Exchangers for Staggered Tube Arrangement'*, International Journal Heat and Mass Transfer, Vol. 41, pp. 425-433, 1998.

[11] S. Acharya, S. Dutta and T.A. Myrum, *'Heat Transfer in Turbulent Flow Past a Surface-Mounted Two-Dimensional Rib'*, Transactions of the ASME, Vol. 120, N°4, pp. 724 - 734, 1998.

[12] S. Acharya, T.A. Myrum, X. Qiu and S. Sinha,, *'Developing and Periodically Developed Flow, Temperature and Heat Transfer in a Ribbed Duct'*, International Journal Heat and Mass Transfer, Vol. 40, N°2, pp. 461-479, 1997.

[13] M. Saffar-Avval and E. Damangir, *'A General Correlation for Determining Optimum Baffle Spacing for all Types of Shell and Tube Exchangers'*, International Journal of Heat and Mass Transfer, Vol. 38, N°13, pp. 501-2506, 1995.

[15] L.C. Demartini, H.A. Vielmo and S.V. Möller, *'Numeric and Experimental Analysis of the Turbulent Flow through a Channel with Baffle Plates'*, Journal of the Brazilian Society of Mechanical Sciences and Engineering, Vol. 26, N°2, pp. 153 - 159, 2004.

[16] A. Tandiroglu,*'Second Law Analysis of Transient Heat Transfer for Turbulent Flow in a Circular Tube with Baffle Inserts'*, International Journal of Exergy, Vol. 2, N°3, pp. 299 - 317, 2005.

[17] Nasiruddin and M.H. Kamran Siddiqui, *'Heat Transfer Augmentation in a Heat Exchanger Tube Using a Baffle'*, International Journal of Heat and Fluid Flow, Vol. 28, N° 2, pp. 318-328, 2007.

[18] Y.G. Lei, Y.L. He, R. Li, Y.F. Gao, *'Effects of Baffle Inclination Angle on Flow and Heat Transfer of a Heat Exchanger with Helical Baffles'*, Chemical Engineering and Processing: Process Intensification, Vol. 47, N°12, pp. 2336-2345, 2008.

[19] R. Karwa, B.K. Maheshwari and N. Karwa, '*Experimental Study of Heat Transfer Enhancement in an Asymmetrically Heated Rectangular Duct with Perforated Baffles'*, International Communication in Heat and Mass Transfer, Vol. 37, N°2, pp. 275-284, 2005.

[20] P. Promvonge. '*Heat Transfer and Pressure Drop in a Channel with Multiple 60° V-baffles'*, International Communication in Heat and Mass Transfer, Vol. 37, N°7, pp. 835-840, 2010.

[22] P. Sriromreun, C. Thianpong and P. Promvonge, '*Experimental and Numerical Study on Heat Transfer Enhancement in a Channel with Z-shaped Baffles*', International Communication in Heat and Mass Transfer, Vol. 39, N°7, pp. 945-952, 2012.

[23] B.K.P. Ary, M.S. Lee, S.W. Ahn and D.H. Lee, '*The effect of the Inclined Perforated Baffle on Heat Transfer and Flow Patterns in the Channel'*, International Communications in Heat and Mass Transfer, Vol. 39, N°10, pp. 1578-1583, 2012.

[24] J.O. Hinze, *'Turbulence'*, McGraw-Hill, 1975.

[25] B.E. Launder, D.B. Spalding, *'The Numerical Computation of Turbulent Flows'*, Computer Methods in Applied Mechanics and Engineering, Vol. 3, N°2, pp. 269-275, 1974.

[26] S.V. Patankar, '*Numerical Heat Transfer and Fluid Flow*', McGraw-Hill, New York, 1980.

[27] J.P. Van Doormaal and G.D. Raithby*, 'Enhancements of the SIMPLE Method for Predicting Incompressible Fluid Flows'*, Numerical Heat Transfer, Vol. 7, N°2, pp. 147-163, 1984.

[28] B.P. Leonard and S. Mokhtari, '*Ultra-sharp Nonoscillatory Convection Schemes for High-Speed Steady Multidimensional Flow*', NASA TM 1-2568, NASA Lewis Research Center, 1990.

[29] M. Mohammadi Pirouz, M. Farhadi, K. Sedighi, H. Nemati and E. Fattahi, *'Lattice Boltzmann Simulation of Conjugate Heat Transfer in a Rectangular Channel with Wall-Mounted Obstacles'*, Scientia Iranica, Vol. 18, N°2, pp. 213-221, 2011.

[30] N. Guerroudj and H. Kahalerras, *'Mixed Convection in a Channel Provided with Heated Porous Blocks of Various Shapes'*, Energy Conversion and Management, Vol. 51, N°3, pp. 505-517, 2010.

[31] S. Sripattanapipat and P. Promvonge, '*Numerical Analysis of Laminar Heat Transfer in a Channel with Diamond-Shaped Baffles*', International Communication in Heat and Mass Transfer, Vol. 36, N°1, pp. 32-38, 2009.

[32] F. Wang, J. Zhang and S. Wang, '*Investigation on Flow and Heat Transfer Characteristics in Rectangular Channel with Drop-Shaped Pin Fins*', Propulsion and Power Research, Vol. 1, N°1, pp. 64-70, 2012.